Axisymmetric contact problem for a flattened cell: contributions of substrate effect and cell thickness to the determination of viscoelastic properties by using AFM indentation

Xinyao Zhu[1], Lanjiao Liu[2], Zuobin Wang[2] and X. Liu[1*]

[1] *School of Engineering, University of Warwick, Coventry CV4 7AL, UK*

[2]*International Research Centre for Nano Handling and Manufacturing of China, Changchun University of Science and Technology, Changchun 130022, China*

Corresponding author: Tel: +44(0)24 765 23136, Fax: Fax: +44(0)24 76 418922

Email: X.Liu@warwick.ac.uk

Abstract

Nanoindentation technology has proven an effective method to investigate the viscoelastic properties of biological cells. The experimental data obtained by nanoindentation are frequently interpreted by Hertz contact model. However, in order to facilitate the application of Hertz contact model, a mass of studies assume cells have infinite thickness which does not necessarily represent the real situation. In this study, a rigorous contact model based upon linear elasticity is developed for the interpretation of indentation tests of flattened cells which represent a factual morphology. The cell, normally bonded to the petri dish, is initially treated as an elastic layer of finite thickness perfectly fixed to a rigid substrate, and the conic indenter is assumed to be frictionless. The theory of linear elasticity is utilized to solve this contact issue and then the solutions are extended to viscoelastic situation which is regarded as a good indicator for mechanical properties of biological cells. To test the present model, an AFM-based creep test has been conducted on living human hepatocellular carcinoma cell (SMMC-7721 cell) and its fullerenol-treated counterpart. The results indicate that the present model could not only describe very well the creep behavior of SMMC-7721 cells, but can also curb overestimation of the mechanical properties due to substrate effect. Moreover, the present model could identify the difference between the control and treated SMMC-7721 cells in terms of the extracted viscoelastic parameters, suggesting its potential in revealing the biomechanical effects of fullerenol-like drug treatment on cancerous cells.

Keywords: Atomic force microscope (AFM); Nanoindentation; Substrate effect; Finite thickness of cell; Viscoelasticity; Creep

1. Introduction

The measurement of viscoelastic properties of living cells can provide important information about the biomechanical effects of drug treatment, diseases and aging. To date, a variety of testing techniques have been used to measure the viscoelastic mechanical properties of biological cells, e.g. micropipette aspiration [1], atomic force microscopy [2], optical tweezers [3, 4] and magnetic tweezers [5]. Compared with other techniques, AFM has many advantages

such as direct interaction with the sample, flexibility in option of probe type and convenient imaging of surface topography of cell. However, AFM-based quantification of the biomechanical property requires an appropriate rheological model which could describe the factual situation of cell indentation. Although Hertz contact model is frequently used to interpret the experimental data obtained by AFM indentation, one of its main assumptions, i.e. treating indented cell as semi-infinite space might be contradicted by the film morphology of cells after being removed from their native environment [6, 7]. In this sense, the estimation of cell properties would be affected by the stiff substrate. If not accounted for, substrate effect would lead to overestimation of the measured parameters [8–10], e.g. elastic modulus, viscosity and diffusion. In this regard, it is essential to develop an effective means to characterize the effect of film thickness in cell indentation.

The indentation of thin layer by spherical indenters has been commonly studied in the literature using either cumbersome numerical calculations or analytical modeling [11–14]. In this sense, Dimitriadis et al. [15] adopted an imaging method to present a convenient correction to Hertz model for thin and elastic film subject to spherical tip indentation. Based on this modification, AFM measurements with spherical tip become a common experimental method to quantify the mechanical properties of spread cells [6, 16]. With a spherical indenter, the measured mechanical properties only represent an average response of a sample, while information of features smaller than size of indenter would be missing [8]. In addition, although Dimitriadis's model has been modified to characterize conical tip indentation [8, 9], there exists inconsistency and non-uniformity between the multiplicative correction factors provided by these studies. In this regard, it is imperative to develop a universal correction to Hertz contact model to account for indentation of thin layers, regardless of size or profile type of the indenter.

In this work, we use linear theory of elasticity to develop a new correction to Sneddon's solutions [17] for a conical tip indentation on thin layer, which could be used to improve the evaluation of the viscoelastic properties of flattened cell by nanoindentation. Meanwhile, an AFM-based creep test is performed on human hepatocellular carcinoma (SMMC-7721 cell), being one of the most common cancer types worldwide, and its fullerenol-treated counterpart. The validity of the present model is demonstrated by fitting it to the experimental data. The extracted viscoelastic parameters by our correction model are compared to the values determined by the conventional Sneddon's solutions to verify that the present model could deal with substrate effect. Moreover, the determined viscoelastic properties of normal SMMC-7721 cells are different from their fullerenol-treated counterparts, suggesting that the biomechanical parameters determined by our correction model could also be used as biomarker to evaluate the effects of fullerenol or other anticancer agents on the cells and thus can represent a crucial part of the potential cancer progression. In addition, it is worth noting that measurements of absolute values of viscoelastic modulus of cell prove a powerful tool to quantify the effect mutations of intracellular scaffolds (i.e. actin cortex) [18]. The semi-analytical dependence of indentation depth on time is given, which is more convenient in practical applications. To the best of our

knowledge, the present study represents a first attempt of applying linear theory of elasticity to flattened cell to quantify its viscoelastic properties.

2. Theoretical Model

2.1 Formulation of elastic film indented by a rigid conic tip

Consider the axisymmetric contact problem of a rigid conic tip on an elastic layer as illustrated in Figure 1. The layer is perfectly bonded to the rigid substrate at the interface $z = h$ while the contact between the indenter and the film is assumed to be frictionless. The cylindrical coordinate (r, φ, z) is used as shown in Figure1, where the origin coincides with the overlapping point between the generatrix of the conic and the upper face of undeformed layer. Under these assumptions, the displacement boundary condition consists of:

$$w = \delta - \Psi(r)(0 \le r \le a, z = 0) \quad (1a)$$

$$w = u = 0(0 \le r < \infty, z = h) \quad (1b)$$

and the stress boundary condition is comprised of:

$$\sigma_z = 0 \ (r > a, z = 0) \quad (2a)$$

$$\tau_{rz} = 0 \ (0 \le r < \infty, z = 0) \quad (2b)$$

where σ_z and τ_{rz} are the normal and tangential stress components respectively and $\Psi(r)$ denotes the axisymmetric shape of the indenter. Since the deformation of the layer subjected to the normal force P is axisymmetric, the radial displacement u and vertical displacement w are independent of the hoop coordinate φ and they satisfy the field equations of the linear theory of elasticity [19] for homogeneous, isotropic materials, given as:

$$(1 - 2\nu)\nabla^2\mathbf{u} + \nabla(\nabla \cdot \mathbf{u}) = 0 \quad (3)$$

where $\mathbf{u} = (u, 0, w)$ is the displacement vector, ν denotes Poisson's ratio and ∇ represents gradient operator.

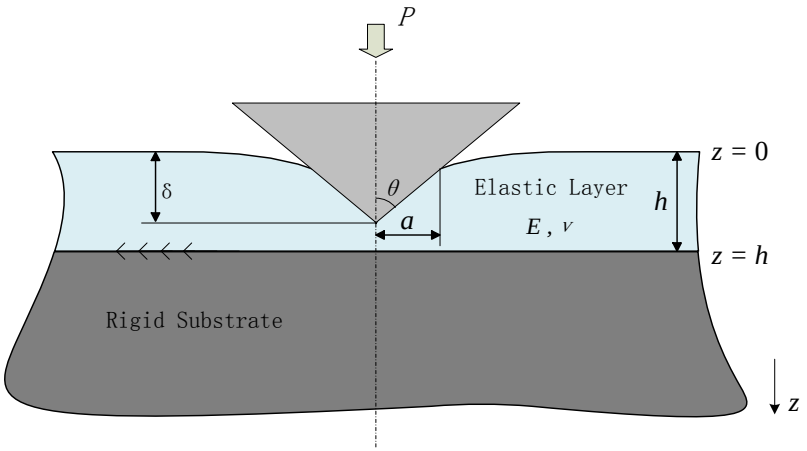

FIGURE 1: Axisymmetric contact between a frictionless conic and an elastic layer perfected bonded to rigid substrate.

The solution of the axisymmetric contact problem depicted in Figure 1 could be solved in terms of Papkovich–Neuber solution for the expression of the components of displacement

vector:

$$2Gu_r = -\frac{\partial}{\partial r}[\Phi_0(r,z) + z\Phi_1(r,z)] \quad (4a)$$

$$2Gu_z = -\frac{\partial}{\partial z}\Phi_0(r,z) - z\frac{\partial}{\partial z}\Phi_1(r,z) + (3-4\nu)\Phi_1(r,z) \quad (4b)$$

and stress vector:

$$\sigma_z = 2(1-\nu)\frac{\partial}{\partial z}\Phi_1(r,z) - \frac{\partial^2}{\partial z^2}\Phi_0(r,z) - z\frac{\partial^2}{\partial z^2}\Phi_1(r,z) \quad (5a)$$

$$\tau_{rz} = \frac{\partial}{\partial r}[(1-2\nu)\Phi_1(r,z) - \frac{\partial}{\partial z}\Phi_0(r,z) - z\frac{\partial}{\partial z}\Phi_1(r,z)] \quad (5b)$$

where Φ_i (i = 0,1) is harmonic function known as the Boussinesq–Papkovitch potential functions [20], and G denotes shear modulus. Since the solution of stress and displacement under the mixed boundary conditions have been developed by many studies [21, 22], its detailed derivation procedure is not repeated in this study. Herein, we directly formulate the dependence of indentation force P and indentation depth δ on the contact radius a as

$$P = \frac{2aE\delta}{1-\nu^2}\int_0^1 \omega(\tau)d\tau \quad (6a)$$

and

$$\delta = -\frac{\pi}{2}a\cot\theta\,\frac{\omega_c(1)}{\omega_f(1)} \quad (6b)$$

respectively, where $\omega(\tau) = \omega_f(\tau) + \pi a\omega_c(\tau)\cot\theta/2\delta$, and $\omega_c(\tau)$ and $\omega_f(\tau)$ are the solutions of the following Fredholm integral equation of the second kind:

$$\omega_c(\xi) + \frac{1}{\pi}\int_{\tau=0}^1 \omega_c(\tau)[K(\tau+\xi) + K(\tau-\xi)]d\xi = -\xi \quad (7a)$$

and

$$\omega_f(\xi) + \frac{1}{\pi}\int_{\tau=0}^1 \omega_f(\tau)[K(\tau+\xi) + K(\tau-\xi)]d\xi = 1 \quad (7b)$$

respectively, in which

$$K(u) = \frac{a}{h}\int_{\alpha=0}^{\infty} \frac{(3-4\nu)e^{-\alpha}sh\alpha - \alpha(1+\alpha) - 4(1-\nu)^2}{\alpha^2 + 4(1-\nu)^2 + (3-4\nu)sh^2\alpha} cos(\frac{\alpha au}{h})d\alpha \quad (8)$$

If the dimensionless parameters

$$\kappa\left(\frac{a}{h},\nu\right) = \int_0^1 \omega(\tau)d\tau \quad (9a)$$

$$\chi\left(\frac{a}{h},\nu\right) = -\frac{\omega_c(1)}{\omega_f(1)} \quad (9b)$$

and

$$\psi\left(\frac{a}{h},\nu\right) = \kappa\left(\frac{a}{h},\nu\right)/\chi\left(\frac{a}{h},\nu\right) \quad (9c)$$

are introduced, equation (6*a*) and equation (6*b*) could be rewritten as

$$P = \frac{\pi E}{1-\nu^2}a^2\cot\theta\cdot\psi(\frac{a}{h},\nu) \quad (10a)$$

and

$$\delta = \frac{\pi a \cdot cot\theta}{2\chi(\frac{a}{h},\nu)} \quad (10b)$$

respectively. The two Fredholm integral equations of the second kind could be solved by numerical method for a given value of *a*/*h* and *v*. Since biological cell is always treated as incompressible, the Possion's ratio *v* equals 0.5, and thus the three dimensionless parameters are only dependent on *a*/*h*. After application of numerical techniques to equation (7*a*) and equation (7*b*), χ and ψ are solved and fitted by polynomials by least square method, formulated as

$$\chi(a/h) = -0.46\left(\frac{a}{h}\right)^3 + 0.28\left(\frac{a}{h}\right)^2 + 0.57\left(\frac{a}{h}\right) + 1 \quad (11a)$$

and

$$\psi(a/h) = -0.26\left(\frac{a}{h}\right)^4 + 0.47\left(\frac{a}{h}\right)^3 - 0.006\left(\frac{a}{h}\right)^2 + 0.0003\left(\frac{a}{h}\right) + 0.5 \quad (11b)$$

respectively, whose fitting results are plotted in Figure2. Eliminating *a* in equation (10*a*) and (10*b*) could result in

$$P = \frac{2E\delta^2 tan\theta}{\pi(1-\nu^2)} \cdot 2\chi^2\psi \quad (12)$$

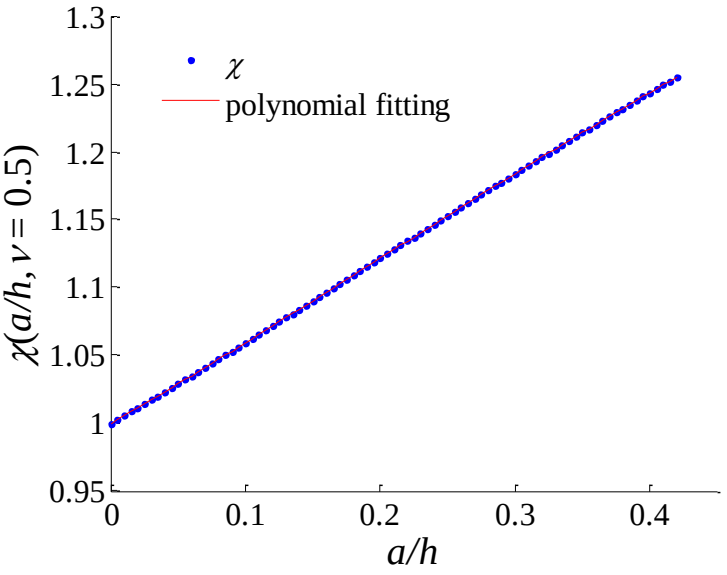

(*a*)

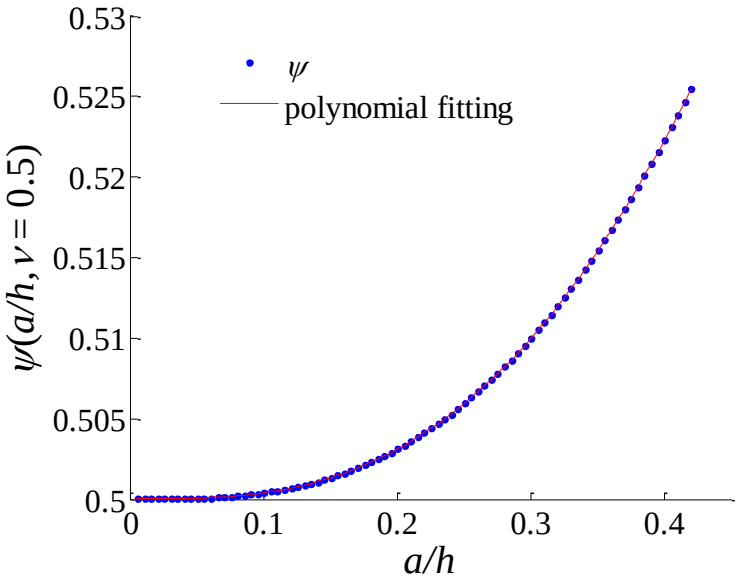

(*b*)

FIGURE 2: Polynomial fitting results of (*a*) $\chi(a/h, \nu = 0.5)$ and (*b*) $\psi(a/h, \nu = 0.5)$.

2.2 Viscoelastic Situation

The viscoelastic behavior of materials can be simulated by the *standard solid* [23], which is shown in Figure 3. It is comprised of an elastic spring, which describes an instantaneous elastic deformation, placed in series with a parallel combination of a spring and dashpot, which describes a delayed elastic deformation. The stress σ applied on the spring element is proportional to its strain ε, i.e. $\sigma = E\varepsilon$, while the stress on the dashpot element is proportional to the rate of its strain, i.e. $\sigma = \eta \cdot d\varepsilon/dt$. The coefficient E and η denote elastic modulus and viscosity respectively. For the constitution shown in Figure 3, the corresponding constitutive relation is given as

$$\sigma + \frac{\eta}{E_1+E_2}\frac{d\sigma}{dt} = \frac{E_1E_2}{E_1+E_2}\varepsilon + \frac{\eta E_2}{E_1+E_2}\frac{d\varepsilon}{dt} \quad (13)$$

where E_1 and E_2 denote the two spring constants. If the stress σ is a unit Heaviside step function $\sigma = H(t)$, the corresponding output strain is termed creep compliance $J(t)$, given as:

$$J(t) = \frac{1}{E_2} + \frac{1-e^{-t/\tau}}{E_1} \quad (14)$$

where $\tau = \eta/E_1$, termed characteristic retardation time corresponding to the time during which the sample deforms by $1\text{-}e^{-1}$ (or 63.2%) of the total creep deformation. It can be seen from equation (14) that $J(0^+) = 1/E_2$, and $J(\infty) = 1/E_1 + 1/E_2$. Therefore, the *standard solid* model has an instantaneous modulus $E_0 = E_2$ and equilibrium modulus $E_\infty = E_1E_2/(E_1+E_2)$. It should be pointed out that the *standard solid* model is a relatively universal model and it covers two extreme cases. For example, as $E_2 \to \infty$, Figure3 degrades to a spring in parallel with a dashpot (Kelvin model) whilst as $E_1 \to 0$, *standard solid* model reduces to a spring in series with a dashpot (Maxwell model).

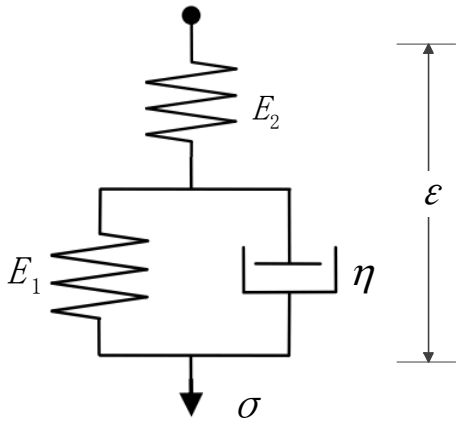

FIGURE 3: Schematic diagram of standard solid model where a first spring (whose stiffness is E_1) is in parallel with a dashpot and then connected with a second spring (whose stiffness is E_2).

For the viscoelastic situation, both Lee and Radok [24] and Ting [25] offered a general solution to linear viscoelastic Boussinesq problem (an infinite half-space indented by an arbitrary shape of rigid, axisymmetric and frictionless punch) as long as the contact radius is non-decreasing as mutual approach increases. According to their theory, substituting the elastic modulus in the Sneddon's solutions with the modulus-displacement convolution in the time domain leads to the relationship between the contact radius a and the applied force F as [26, 27]:

$$a^2(t)\psi(\frac{a}{h}) = \frac{1-\nu^2}{\pi} tan\theta \cdot J(t) * F(t) \quad (15)$$

where the asterisk denotes convolution, i.e.

$$J(t) * F(t) = \int_{\xi=0^-}^{t} J(t-\xi)\frac{d}{d\xi}F(\xi)d\xi \quad (16)$$

Performing Laplace transform on both sides of equation (16) yields

$$\mathcal{L}[a^2(t)\psi(\frac{a}{h})] = \frac{1-\nu^2}{\pi} tan\theta \mathcal{L}[J(t)]\mathcal{L}[\frac{dF(t)}{dt}] \quad (17)$$

If $F(t)$ is assumed to be an Heaviside step function, one has

$$\mathcal{L}[a^2(t)\psi(\frac{a}{h})] = \frac{1-\nu^2}{\pi} tan\theta \mathcal{L}[J(t)]F_{max} \quad (18)$$

Performing inverse Laplace transform on equation (18) results in

$$[\frac{a(t)}{h}]^2 \psi[\frac{a(t)}{h}] = \frac{1-\nu^2}{\pi} J(t)\frac{F_{max}}{h^2} \cdot tan\theta \quad (19)$$

On the other hand, the time-dependent indentation $\delta(t)$ and contact radius $a(t)$ are also related by equation (10*b*), i.e.

$$\delta(t) = \frac{\pi a(t)\cdot cot\theta}{2\chi[\frac{a(t)}{h}]} \quad (20)$$

Therefore, the dependence of indentation depth $\delta(t)$ on time could be derived by solving equation (19) and substituting $a(t)$ into equation (20), which is ready for fitting the δ–t curve

obtained by experiment.

3. Materials and Methods

To validate the present model, AFM-based creep tests have been performed on SMMC-7721 cell.

3.1 Cell Preparation

SMMC-7721 cells were revived after being frozen in freezer and was incubated in Roswell Park Memorial Institute (RPMI)-1640 media with 10% of fetal bovine serum (FBS) and antibiotics (penicillin-streptomycin solution). The protocol for the culture and fullerenol treatment of SMMC-7721 cells have been described in details elsewhere [28].

3.2 Atomic Force Microscopy

The module of the AFM employed in this study is JPK NanoWizards 3 BioScience (Berlin, Germany), and it is mounted on an inverted optical microscope (Olympus IX71; Tokoy, Japan), allowing the AFM and optical microscope imaging simultaneously. The criterion for cantilever selection is that the compliance of the cantilever should be within the range of the sample compliance. For very soft and delicate cells, the softest cantilevers are available with spring constants ranging from 0.01 to 0.06 *N*/*m* (JPK Application Note). Before indentation, the spring constant of the AFM cantilever was calibrated. A silicon nitride cantilever whose spring constant is 0.059 *N/m* after calibration, was used for cell-tip indentation in this work. The probe is a square pyramid tip with a half-opening angle of $\alpha = 25°$ (half-angle to face), and its radius and height are 10 *n*m and 4 μm respectively, as can be seen in Fig. 4 (*c*) and (*d*).

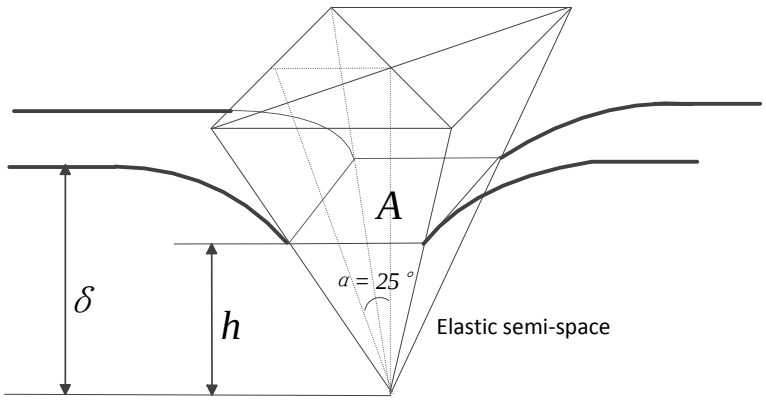

(*a*)

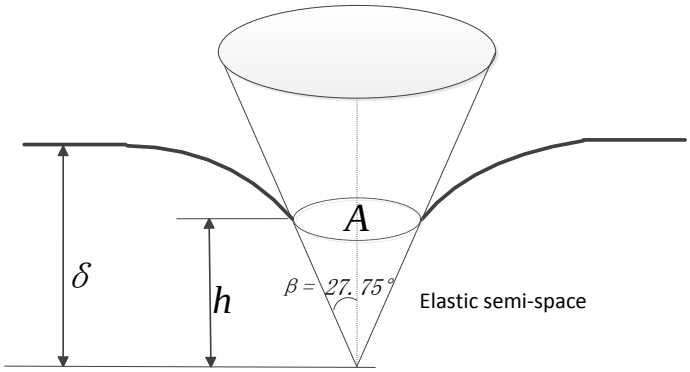

(*b*)

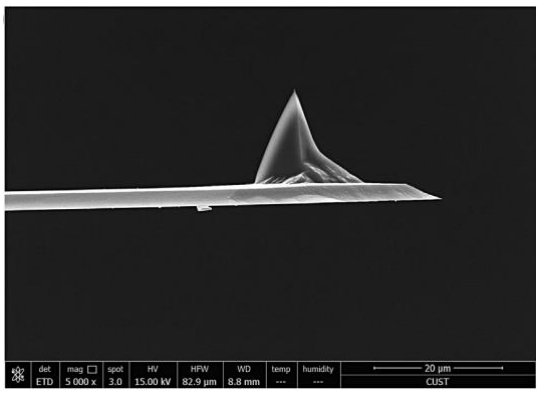

(*c*)

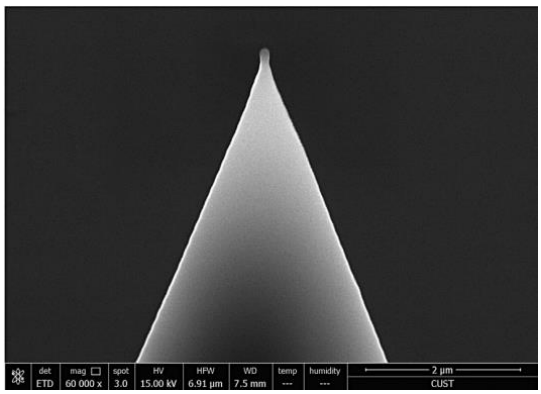

(*d*)

FIGURE 4: Schematic of a compliant semi-infinite space indented by (*a*) a square pyramid and (*b*) a conic indenter. α and β denote the half-opening angle of the pyramid and conic indenter respectively.

Figure 4(*a*) shows schematically that the displacement of a pyramid tip along a distance δ inwards a half-space material creates a tip-material contact area, which is determined by the contact depth *h*. Since the AFM cantilever tip is a pyramid, the projection area *A* of the tip-sample contact surface is not circular, i.e. not axisymmetric. However, numerical analysis [29, 30] indicates that Figure 4(*a*) could be approximated by the contact between a conic indenter and substrate material as illustrated in Figure 4(*b*) with a negligible error of 0.012, as long as the conic gives the same projected area-to-depth ratio *A*/*h* as that of pyramid. In this regard, the half-opening angle β of the conic equals 27.75°in order to retain the same area-to-depth ratio of pyramid shown in Figure 4(*a*).

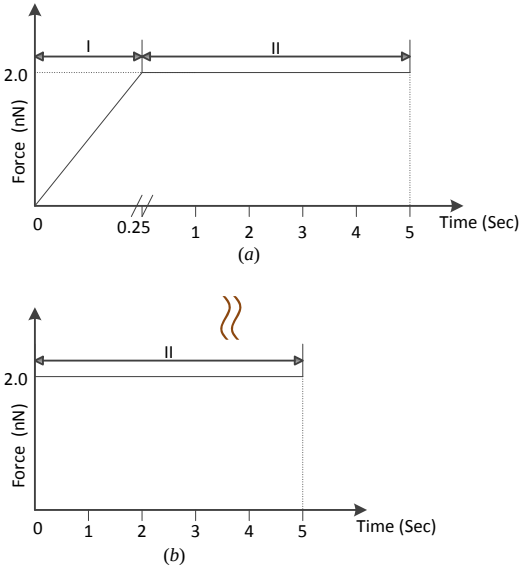

FIGURE 5: Schematic of the AFM indentation force versus time (*a*) and its approximation (*b*) by Heaviside step function.

3.3 Loading method

The determination of viscoelastic properties of material is commonly realized by the creep response to a prescribed load. The loading method of indentation force illustrated in Figure5 is to realize the creep test on single cells. Figure 5(*a*) depicts the factual loading history, which could be approximated by an Heaviside step function as shown in Figure 5(*b*), as long as the loading period (stage I) is smaller than one tenth of that of dwelling period (stage II) [12]. In the present AFM-based creep test, the creep tests were conducted by constant force delay mode where the force reaches its maximum value (2 *nN*) within 0.25 seconds and resides at the peak value for 5 seconds.

4. Results and discussions

4.1 Cell topography analysis

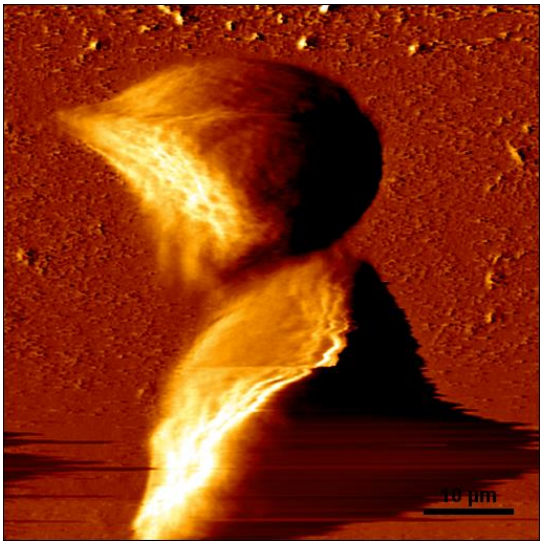

(*a*)

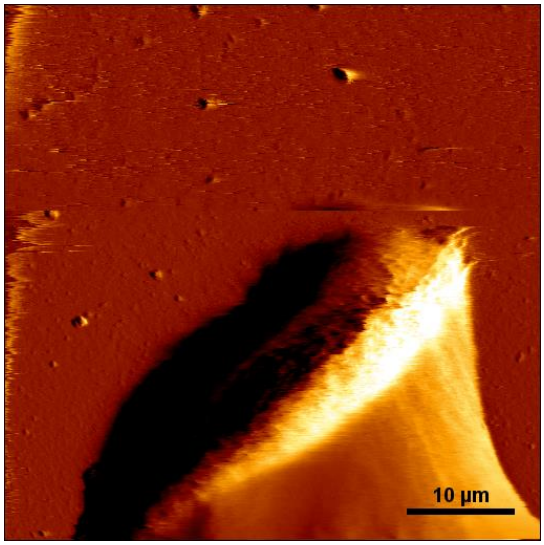

(*b*)

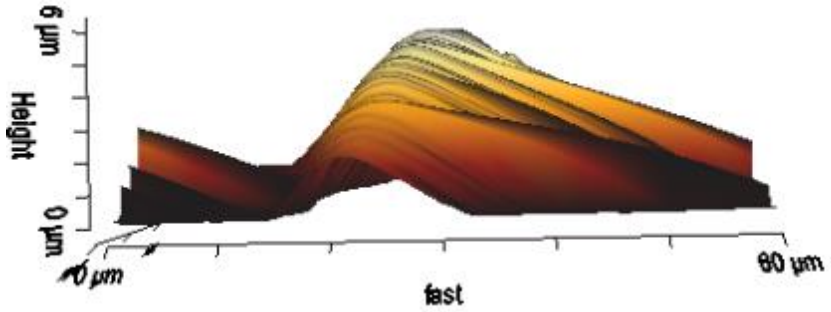

(*c*)

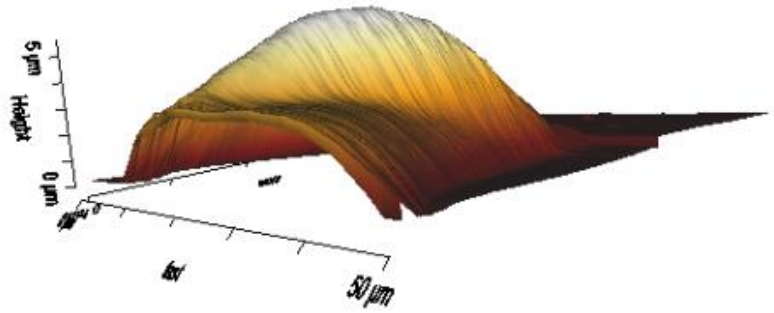

(*d*)

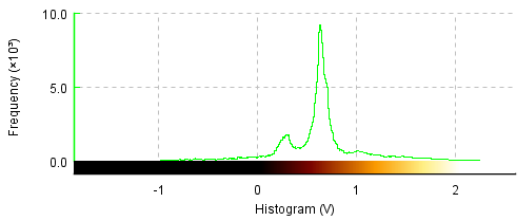

(*e*)

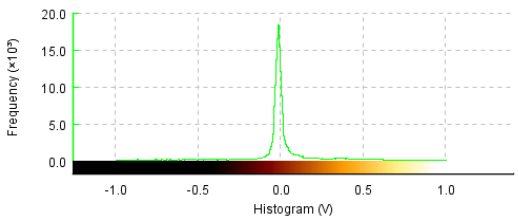

(*f*)

FIGURE 6: (*a*) and (*b*) represent AFM deflection image of control and treated cells respectively. (*c*) and (*d*) denote the

3D distribution of cell height for control and treated cells respectively. (*e*) and (*f*) are the corresponding statistics of cell height value for control and treated cells respectively.

Priority to creep test, the contact mode of AFM was used for topography imaging of the cells. The AFM deflection images of both control (Figure6 (*a*)) and treated cell (Figure 6(*b*)) were obtained by the AFM contact imaging mode in real-time. The majority of control cell shape are polygonal (Figure 6(*a*)) whist after being treated by fullerenol, the SMMC-7721 cell exhibits a significant change from polygon to shuttle as shown in Figure 6(*b*). In addition, the AFM deflection imaging can also enable us to investigate the height distribution of individual cells. The 3D view of cell topography (Figure 6(*c*) and (*d*)) indicates that both control and treated cells spread above the substrate, which is further confirmed by the histogram (Figure 6(*e*) and (*f*)) of pixel value where the narrow range suggests that the cell is fairly flat. The statistical analyses of the cell height and surface roughness of the control and treated cells are shown in Figure 7. Significant increase in the mean height after fullerenol treatment could be observed while there is no conspicuous variations in the surface roughness between the two types of cells.

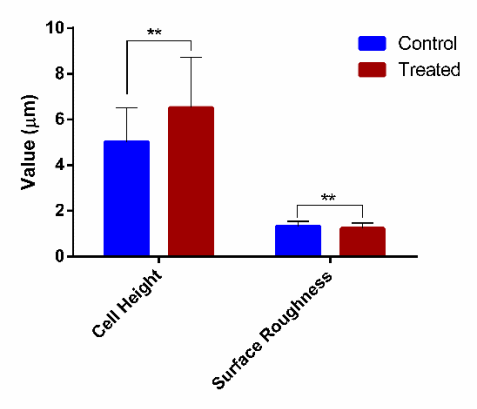

FIGURE 7: The statistics results of cell height and surface roughness. Data are expressed as mean ±SEM of more than 30 cells from 3 separate experiments, where key significances are shown, $^{**}p < 0.01$.

4.2 Analysis of creep test curves

Although the elastic modulus is frequently used to characterize the mechanical properties of biological cells, it does not present a complete description. It can be seen from the blue bold curve in Figure 8 that the cell exhibits a time-dependent deformation under the invariant indentation force, i.e. they creep. Therefore, it is more appropriate to treat the cell as viscoelastic. The mechanical response of the cell to the applied force ranges on a time scale of several seconds, which is very slow compared with the loading time. Therefore, the mechanical response of the cell is divided into two components: an instantaneous, elastic response and a delayed elastic response due to creep deformation. In this study, *standard solid* model of viscoelasticity theory is used to describe the mechanical response of the cell, which is characterized by three parameters: instantaneous modulus E_0, equilibrium modulus E_∞ and

viscosity η, as introduced by equation (13) and Figure 3. Since SMMC-7721 cell spreads like film as analyzed in Sect. 4.1, the present contact model developed in Sect. 2 is justified for fitting process, in which the local thickness of the indented point was estimated by the AFM deflection imaging function as mentioned in Sect. 4.1. For the purpose of comparison, Sneddon's solutions are also used for fitting where the cell is treated as semi-infinite space. We find that the fits of these two models to the creep deformation data are very good regardless of the cell type, as can be seen in Figure 8, with coefficient of determination close to one ($R^2 \geq 0.93$).

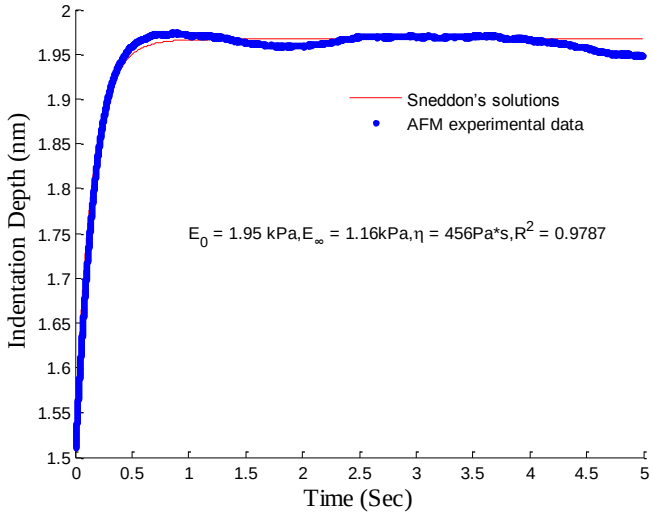

(*a*)

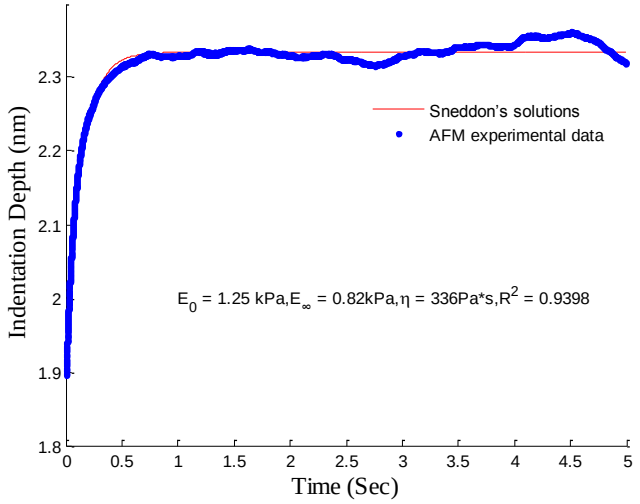

(*b*)

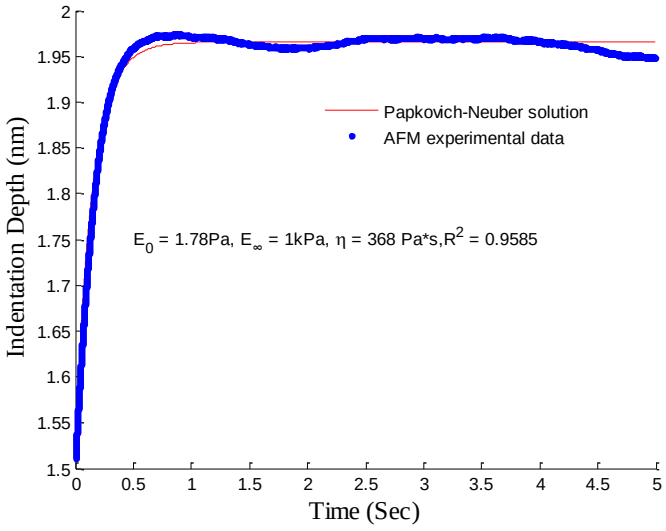

(*c*)

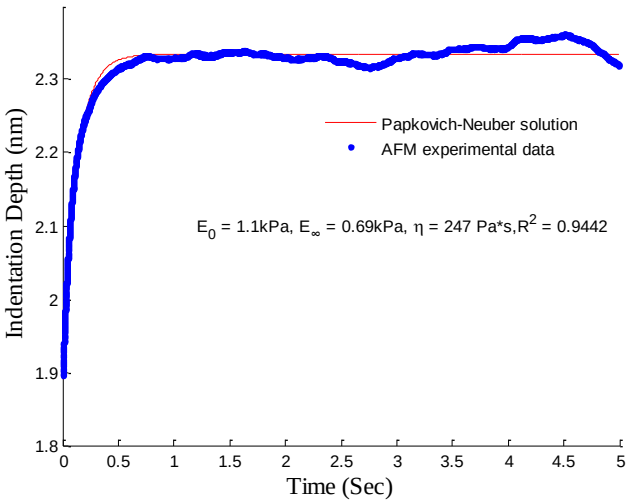

(*d*)

FIGURE 8: Fitting results of control cells ((*a*) and (*c*)) and treated cells ((*b*) and (*d*)) by the two models.

4.3 Cell Viscoelastic Properties

The viscoelastic parameters of control and treated cells were determined according to Sneddon's solutions and the present model, and their mean values are presented in Figure9. In the present model, the value of cell thickness is determined by the AFM deflection imaging. It can be seen that the three parameters determined by the present model are lower than that determined by the Sneddon's solutions, regardless of the cell type, which indicates that the present model could alleviate the overestimation of biomechanical properties by Sneddon's solutions.

From Figure 9, it could be also seen that the average elastic modulus and viscosity of the treated cells show a diminishing trend compared to those control cells, regardless of whichever model adopted. Concretely, control cells have significant higher ($P < 0.01$) instantaneous

modulus and viscosity than the instantaneous modulus and viscosity of treated cells, while the equilibrium modulus of control cell is slightly higher that its treated counterpart. Previous studies have already reported that both elasticity and viscosity are heavily impacted by the levels and organization state of actin cortex [31]. Since actin cortex are transformed into actin aggregates and distributed irregularly within the cells after being treated by fullerenol [32], we infer that this transform of actin cortex induces variation of the viscoelastic parameters of SMMC-7721 cells.

In our study, we treat the cell as a homogeneous material and thus present a global equivalent quantification of viscoelastic properties of the cell. We admit that the assumption of homogeneity is a limitation in our present work, and inhomogeneous model would present more details. For example, Feneberg et al. [33] measured shear elasticity of cell envelops using magnetic tweezer technique, which is important in terms of providing insight into the structure of cell envelops or cytoplasm.

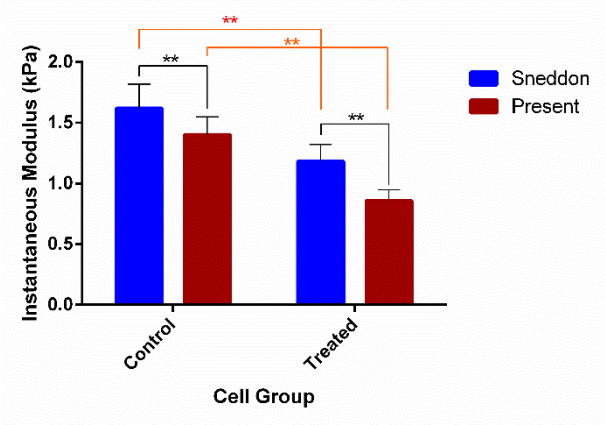

(*a*)

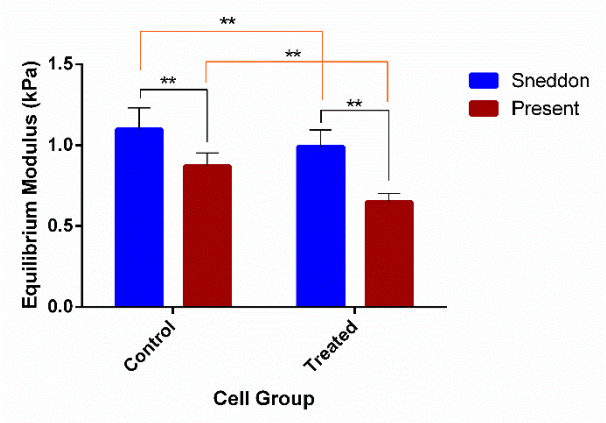

(*b*)

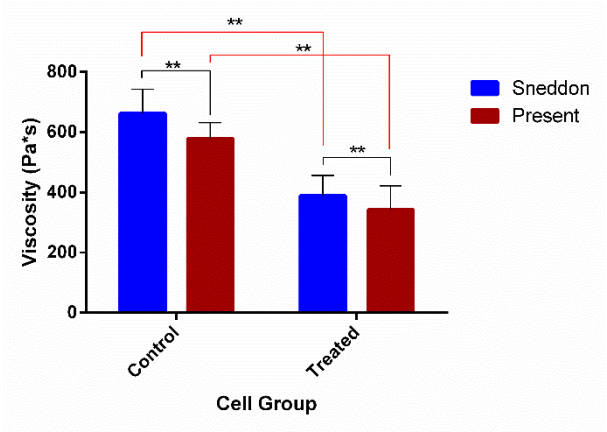

(*c*)

FIGURE 9: The statistics results of (*a*) E_0 , (*b*) E_∞ and (*c*) η. Data are expressed as mean ±SEM of more than 30 cells from 3 separate experiments, where key significances are shown, **p<0.01.

4.4 Validation and comparison

In order to further validate the capability of the present model in alleviating the substrate effect, we present a test of it on different height area of cell as elaborated follows. As shown in Figure 10(*a*), we select an arbitrary intersecting surface and plot the variation of cell height along the cut path. Creep tests are performed along the path and the indentation depth-time curves are fitted by both models. The variation of the instantaneous modulus (E_0) and the equilibrium modulus E_∞ along the cutting path is plotted in Figure 10(*c*) and (*d*) respectively. At the nucleus region ($10 < x < 20$ μm), the determined elastic moduli exhibit uniformity, indicating material homogeneity in this area. In the region around the nucleus ($5 < x < 10$ μm & $22 < x < 30$ μm), there exists actin filaments network which plays a key role in cellular mechanical stability, and therefore we observe increase of elastic modulus in this area. At the margin of the cell ($0 < x < 5$ μm & $30 < x < 34$ μm), the elastic modulus decreases since the density of actin filaments declines in this area. In all regions, the Sneddon's solutions result in higher elastic modulus compared to the present model. In the nucleus region where the local thickness is high, the ration δ/H is low, and thus one gets low value of the correction factor in equation (12), resulting in nearly equal elastic modulus predicted by the two models. The substrate effect becomes significant at the margin area, where the multiplicative factor dominates in equation (12).

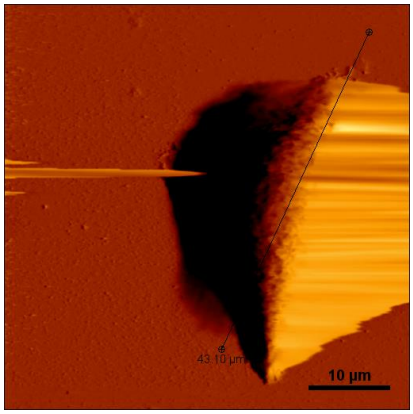
43.10 µm
10 µm

(*a*)

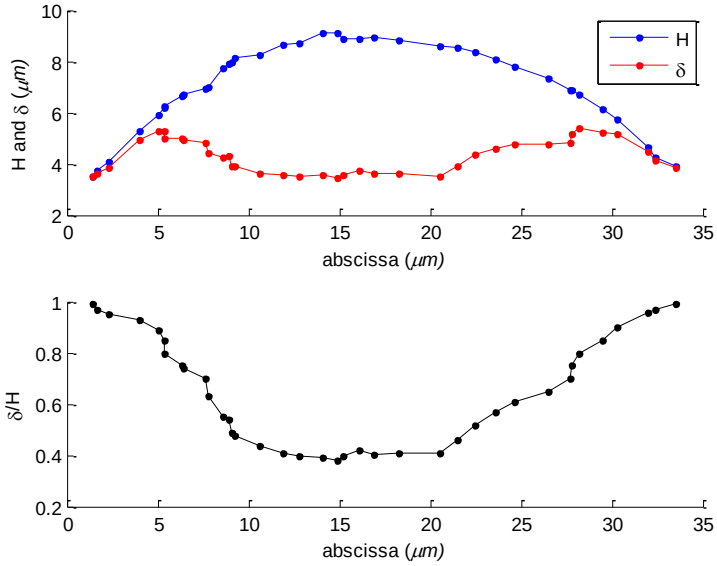
H and δ (µm)
H
δ
abscissa (µm)
δ/H
abscissa (µm)

(*b*)

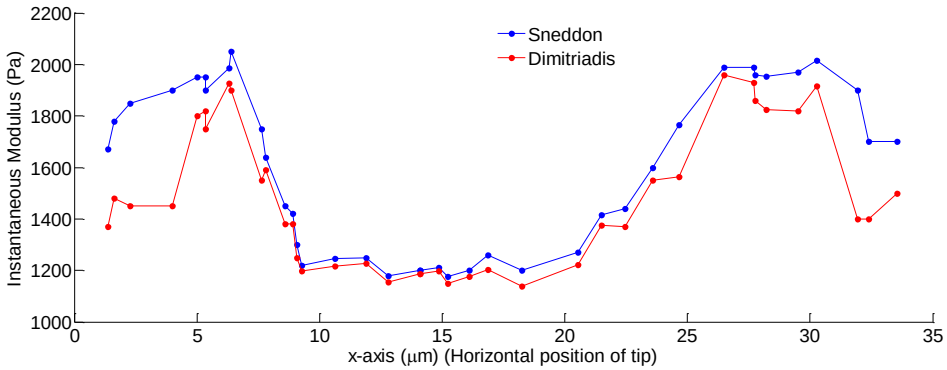
Instantaneous Modulus (Pa)
Sneddon
Dimitriadis
x-axis (µm) (Horizontal position of tip)

(*c*)

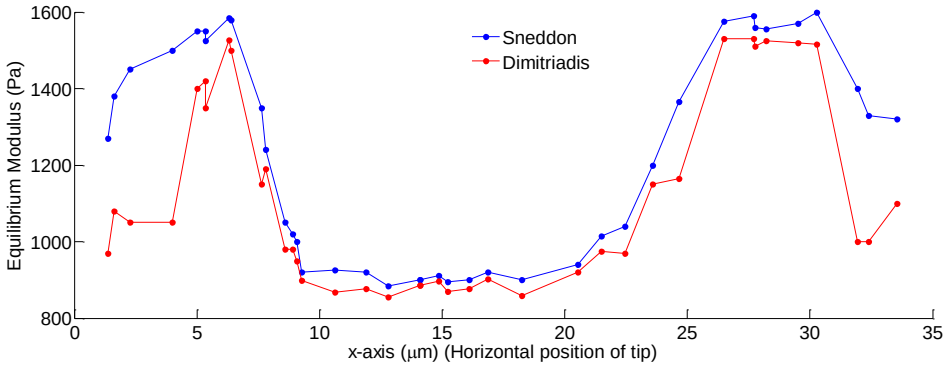

(*d*)

FIGURE 10: (*a*) Deflection image of single control cell with the scanning range of 55×55 μm. (*b*) Cell height profile, indentation depth and δ/H variation along cut path. (*c*) and (*d*) denote elastic moduli variation along cut path.

5. Conclusions

In this paper, we first introduce the present model based on the contact mechanics of thin film, and this model underlies the interpretation of flattened cell subjected to AFM indentation. The present model relieves the major assumption of semi-infinite space of classic Sneddon's solutions to account for the realistic morphology of spread cells. Afterwards, the model is extended to viscoelastic constitution to reflect cell's viscoelastic nature. The AFM-based creep test was conducted to validate the present model. The topography imaging of SMMC-7721 cell confirms the cells exhibit flattened morphology which justifies the application of present model. The fitting results have shown that the present model can not only describe very well the creep behavior of the SMMC-7721 cell, but also avoid the overestimation of elastic and viscosity properties of thin film due to substrate effect. Hereupon, we account for the suppression of overestimation by the present model in terms of correction factor. In addition, the present model could identify the variations of the SMMC-7721 cell and its fullerenol-treated counterpart in terms of the extracted viscoelastic parameters, which reveals its instructive significance in understanding fullerenol-induced effect on the viscoelastic properties of cancerous cells, and the potential in anticancer drug in terms of fullerenol application.

Conflicts and Interest

The authors declare that there is no conflicts of interest within the present study.

Acknowledgements

The authors are grateful for the technical supports from the Laboratory of Precision Engineering and Surfaces of the University of Warwick and the International Research Centre for Nano Handling and Manufacturing, Changchun University of Science and Technology. This project has been partially funded by the European Union's Horizon 2020 research and innovation programme under the Marie Skłodowska-Curie grant agreement No 644971, FP7 MCA-IRSES (612641) and the

China-EU research programme (S2016G4501).

References

[1] R. Zhao, K. Wyss, and C.A. Simmons, "Comparison of analytical and inverse finite element approaches to estimate cell viscoelastic properties by micropipette aspiration," *Journal of Biomechanics*, vol. 42, no. 16, pp. 2768–2773, 2009.

[2] E.M. Darling, S. Zauscher, and F. Guilak, "Viscoelastic properties of zonal articular chondrocytes measured by atomic force microscopy," *Osteoarthritis & Cartilage*, vol. 14, no. 6, pp. 571–579, 2006.

[3] J.P. Mills, L. Qie, M. Dao, et al., "Nonlinear elastic and viscoelastic deformation of the human red blood cell with optical tweezers," *Mechanics & Chemistry of Biosystems Mcb*, vol. 1, no. 3, pp. 169–180, 2004.

[4] D.R. Murdock, S. Ermilov, F. Qian et al., "Optical tweezers study of viscoelastic properties in the outer hair cell plasma membrane," *Proceedings of SPIE*, vol. 5331, pp. 118–125, 2004.

[5] A.R. Bausch, W. Möller, and E. Sackmann, "Measurement of Local Viscoelasticity and Forces in Living Cells by Magnetic Tweezers," *Biophysical Journal*, vol. 76, no.1, pp. 573–579, 1999.

[6] E.M. Darling, S. Zauscher, J.A. Block, and F. Guilak, "A thin-layer model for viscoelastic, stress-relaxation testing of cells using atomic force microscopy: do cell properties reflect metastatic potential," *Biophysical Journal*, vol. 92, no. 5, pp. 1784–1791, 2007.

[7] J. Chen, "Nanobiomechanics of living cells: a review," *Interface Focus A Theme Supplement of Journal of the Royal Society Interface*, vol. 4, no. 2, pp. 20130055, 2012.

[8] J.A.C. Santos, L.M. Rebêlo, A.C. Araujo et al., "Thickness-corrected model for nanoindentation of thin films with conical indenters," *Soft Matter*, vol. 8, no. 16, pp. 4441–4448, 2012.

[9] N. Gavara, and R.S. Chadwick, "Determination of the elastic moduli of thin samples and adherent cells using conical atomic force microscope tips," *Nature Nanotechnology*, vol. 7, no. 11, pp. 733–736, 2012.

[10] J. Sanchez-Adams, R.E. Wilusz, and F. Guilak "Atomic force microscopy reveals regional variations in the micromechanical properties of the pericellular and extracellular matrices of the meniscus," *Journal of Orthopaedic Research*, vol. 31, no. 8, pp. 1218–1225, 2013.

[11] J. Ogilvy, “A parametric elastic model for indentation testing of thin films,” *Journal of Physics D Applied Physics*, vol. 26, no. 12, pp. 2123–2131, 1998.

[12] F. Yang, “Indentation of an incompressible elastic film,” *Mechanics of Materials*, vol. 30, no. 4, pp. 275–286, 1998.

[13] R. S. Chadwick, “Axisymmetric indentation of a thin incompressible elastic layer,” *Siam Journal on Applied Mathematics*, vol. 62, no. 5, pp. 1520–1530, 2002.

[14] B. Oommen, and K.J. Van Vliet, “Effects of nanoscale thickness and elastic nonlinearity on measured mechanical properties of polymeric films,” *Thin Solid Films*, vol. 513, no. 1, pp. 235–242, 2006.

[15] E.K. Dimitriadis, F. Horkay, J. Maresca et al., “Determination of elastic moduli of thin layers of soft material using the atomic force microscope,” *Biophysical Journal*, vol. 82, no. 5, pp. 2798–2810, 2002.

[16] S. Vichare, S. Sen, and M.M. Inamdar, “Cellular mechanoadaptation to substrate mechanical properties: contributions of substrate stiffness and thickness to cell stiffness measurements using AFM,” *Soft Matter*, vol. 10, no. 10, pp. 1174–1181, 2014.

[17] I. N. Sneddon, “The relation between load and penetration in the axisymmetric Boussinesq problem for a punch of arbitrary profile,” International Journal of Engineering Science, vol. 3, no. 1, pp. 47–57, 1965.

[18] M. Schindl, E. Wallraff, B. Deubzer, et al., "Cell-substrate interactions and locomotion of Dictyostelium wild-type and mutants defective in three cytoskeletal proteins: a study using quantitative reflection interference contrast microscopy," Biophysical Journal, vol. 68, no. 3, pp. 1177–1190, 1995.

[19] G.M.L. Gladwell, *Contact Problems in the Classical Theory of Elasticity*, Sijthoff and Noordhof, New York, 1980.

[20] A.E. Green, and W. Zerna, *Theoretical elasticity*, Oxford University Press, Oxford, UK, 1954.

[21] W.C. Hayes, L.M. Keer, G. Herrmann, and L.F. Mockros, “A mathematical analysis for indentation tests of articular cartilage,” *Journal of Biomechanics*, vol. 5, no. 5, pp. 541–551, 1974.

[22] S.T. Choi, “Extended JKR theory on adhesive contact of a spherical tip onto a film on a substrate,” *Journal of Materials Research*, vol. 27, no. 1, pp. 113–120, 2012.

[23] W.N. Findley, and F.A. Davis, *Creep and relaxation of nonlinear viscoelastic materials*, MA: Courier Corporation, North Chelmsford, UK, 2013.

[24] E.H. Lee, and J.R.M. Radok, “The contact problem for viscoelastic bodies,” *Journal of Applied Mechanics*, vol. 27, no. 3, pp. 438–444, 1960.

[25] T.C.T. Ting, “The Contact Stresses Between a Rigid Indenter and a Viscoelastic Half-Space,” *Journal of Applied Mechanics*, vol. 33, no. 4, pp. 845–854, 1966.

[26] X.Y. Zhu, E.Siamantouras, K.K. Liu, and X.P. Liu, “Determination of work of adhesion of biological cell under AFM bead indentation,” *Journal of the Mechanical Behavior of Biomedical Materials*, vol. 56, no. 5, pp. 77–86, 2016.

[27] X.Y. Zhu, Z.B. Wang, and X.P. Liu, “Investigation of effect of fullerenol on viscoelasticity properties of human hepatocellular carcinoma by AFM-Based creep tests,” *Journal of Materials Research*, Published (DOI: 10.1557/jmr.2017.229), 2017.

[28] X.Y. Zhu, N. Zhang, Z.B.Wang, and X.P. Liu, “Investigation of work of adhesion of biological cell (human hepatocellular carcinoma) by AFM nanoindentation,” *Journal of Micro-Bio Robotics*, vol. 11, no. 1, pp. 47–55, 2016.

[29] R.B. King, “Elastic analysis of some punch problems for a layered medium,” *International Journal of Solids and Structures*, vol. 23, no. 12, pp. 1657–1664, 1987.

[30] J.M. Antunes, L.F. Menezes, and J.V. Fernandes, “Three-dimensional numerical simulation of Vickers indentation tests,” *International Journal of Solids and Structures*, vol. 43, no. 3, pp. 784–806, 2006.

[31] A.N. Ketene, P.C. Roberts, A.A. Shea et al., “Actin filaments play a primary role for structural integrity and viscoelastic response in cells,” *Integrative Biology Quantitative Biosciences from Nano to Macro*, vol. 4, no. 5, pp. 540–549, 2012.

[32] S.N. Rubtsova, R.V. Kondratov, P.B Kopnin, et al., “Disruption of actin microfilaments by cytochalasin D leads to activation of p53,” *FEBS Letters*, vol. 430, no. 3, pp. 353–357, 1998.

[33] W. Feneberr, M. Aepfelbacher, E. Sackmann, "Microviscoelasticity of the Apical Cell

Surface of Human Umbilical Vein Endothelial Cells (HUVEC) within Confluent Monolayers," Biophysical Journal, vol. 87, no. 2, pp. 1338–1350, 2004.